



Synthesis of microcrystalline indium (III)-MOF and adsorptive and selective removal of dyes

Ketan Maru¹ · Sarita Kalla² · Arup K. Ghosh¹ · Ritambhara Jangir¹

Received: 31 August 2023 / Accepted: 2 October 2023 / Published online: 17 October 2023
© The Author(s), under exclusive licence to Springer Nature B.V. 2023

Abstract

Dye pollution is a significant environmental catastrophe, and it has so far proven to be challenging to purify dye-contaminated water effectively. Metal–organic frameworks (MOFs) have potential of removing dyes from wastewater but effectively addressing the simultaneous removal of multiple dyes remains a challenging task. In-MOF, synthesized in the round-bottom flask, sealed glass tubes, and under microwave conditions, exhibits excellent adsorption for cationic dyes. The identification and characterization of In-MOF were accomplished using several analytical techniques, including Powder X-ray diffraction, Fourier-transform infrared spectroscopy, Brunauer–Emmett–Teller analysis, Thermogravimetric analysis, Scanning electron microscope, Energy-dispersive X-ray spectroscopy, Elemental analysis, and Density functional theory for structure elucidation. In-MOF exhibits outstanding dye removal efficiency for Methylene Blue (MB: 98%; 18.6 mg/g), Azure A (AZA: 99%; 22.4 mg/g), Azure B (AZB: 98%; 17.2 mg/g), Toluidine Blue O (TOLO: 99%; 20.6 mg/g), Rhodamine B (RHB: 82%; 8.8 mg/g), and Congo red (CR: 93%; 14.2 mg/g) individually. Moreover, In-MOF demonstrates remarkable selectivity towards MB removal even in the presence of RHB. The kinetics of adsorption and reusability tests for MB indicate consistent removal capacity for the initial three cycles, but a significant decline of up to 52% is observed by the sixth cycle. These findings establish In-MOF as a promising candidate for industrial applications due to its high removal efficiency and practical synthetic approach.

Keywords In-MOF · Dye removal · Adsorption · Synthetic strategy · Selectivity

Introduction

Water pollution, a significant issue resulting from industrialization, has led to the increasing importance of water purification as a key societal concern [1–4]. This necessitates the implementation of sustainable development strategies to prevent the depletion of current natural resources [5]. Among the various pollutants, organic

dyes play a significant role in the degradation of water quality. Industries such as textile, leather, paper, and printing make extensive use of organic dyes, however, a majority of these dyes are discharged into water bodies as effluent [6, 7]. Dyes such as Methylene Blue (MB), Azure A (AZA), Azure B (AZB), Toluidine Blue O (TOLO), Rhodamine B (RHB), and Congo red (CR) (Fig. S1) are frequently used in the textile, paper, and paint industries. Unfortunately, their discharge into water bodies can cause significant harm to the ecosystem. In general, wastewater concentrations of these dyes typically range from 1 to 50 ppm [8]. Studies have demonstrated that these dyes possess carcinogenic, teratogenic, and mutagenic properties, hence it is essential to remove them from water bodies to safeguard human health [9].

Removal of organic dyes from wastewater is a significant challenge in the field of environmental remediation [10]. Various treatment methods have been proposed, such as adsorption, precipitation, photocatalysis, electrochemical processes, oxidation, ultrafiltration, ozonation, and membrane filtration [11–14]. Particularly, the adsorption technique has been widely recognized as an efficient and practical method for removing dyes from polluted water. Recent research has highlighted the efficacy of various adsorbents [15, 16], including covalent organic frameworks (COFs) [17], zeolites [18], activated carbon [19], biomass [20], and chitosan [21], in removing dyes from wastewater. These materials possess high surface areas and demonstrate selective adsorption of organic dyes, leading to their effective removal. However, they suffer from certain limitations such as prolonged contact time, lengthy activation periods, low water stability, and complex synthesis routes [22–25]. In particular, COFs are impractical for use as adsorbents due to their low quantity of production [26], while zeolites and activated carbon suffer from low reusability and expensive regeneration processes [27]. MOFs, on the other hand, are known for their extraordinary properties, which include a large surface area, impressive selectivity, effective dye removal capacity, exceptional thermal stability, and insolubility in water. These characteristics have established MOFs as a widely recognized and commonly utilized adsorbent for dye removal [14].

The field of Metal–organic frameworks (MOFs) has witnessed significant progress in synthesizing and employing them for the selective removal of dyes [28, 29]. The synthesis of MOFs offers a wide range of possibilities, resulting in diverse structures [30–33]. These structures can vary from well-formed crystals with high structural integrity to hollow structures, analogous structures, core–shell geometries, or mixed structures lacking precise organization, leading to structural heterogeneity [34–36]. Unconventional MOFs, including amorphous, disordered, glass, and liquid MOFs, have also been reported, characterized by the absence of well-arranged crystal structures while still being classified as MOFs [37, 38]. Computational chemistry plays a pivotal role in unravelling the structures of these MOFs with unconventional characteristics [39]. Recent studies have demonstrated the potential of the Three-dimensional electron diffraction (3D-ED) and Continuous rotation electron diffraction (cRED) techniques in elucidating their structures by diffraction of microcrystals. However, it is important to note that this method is still in the research phase and not yet widely accessible [39, 40].

In this regard, the synthesized In-MOF [In₂(BTA)₂μ-NO₃·8H₂O] with its disordered structure and microcrystalline nature emerges as an exceptionally effective

and practical adsorbent for dye removal. Its outstanding attributes include straightforward synthesis, remarkable reusability, and facile regeneration processes, making it a promising candidate for efficient dye adsorption. In-MOF microcrystals exhibit high water stability, insolubility, and strong selectivity for dye removal, making them a highly promising candidate for wastewater remediation applications. Notably, the In-MOFs green synthesis option further enhances its appeal for sustainable wastewater treatment. The superiority of MOFs in dye removal over conventional adsorbents has been extensively established in the literature [41, 42], with the first study by Jung et al. demonstrating the efficacy of MOFs in cationic dye removal in 2010 [43]. Since then, numerous research groups have validated the superior selectivity and capacity of MOFs in dye removal, emphasizing their potential for practical application in wastewater treatment [44–49]. Notably, Morsali et al. reported the synthesis of a multinuclear cluster-based Fe-MOF, which demonstrates efficacy in removing cationic dyes while also exhibiting selective dye removal capabilities. Their study highlighted the potential of Fe-MOF as a promising sorbent for dye removal applications [50]. Furthermore, Sun et al. explored the use of JUC-210, a specific MOF, for the removal of cationic dyes. The research demonstrated the effectiveness of JUC-210 in removing cationic dyes from aqueous solutions [51]. These studies provide valuable insights into the utilization of MOFs for dye removal, emphasizing the importance of selective dye removal and the potential of MOFs as effective sorbents in addressing dye contamination issues.

In this study, an In-MOF, specifically $[\text{In}_2(\text{BTA})_2\mu\text{-NO}_3\cdot 8\text{H}_2\text{O}]$ (In-MOF), was produced using a simple synthetic method involving Indium salt and benzene-1,2,4,5-tetracarboxylic acid in a sealed glass vial. The synthesis was also repeated in RBF and microwave-assisted conditions, with similar results obtained. Computational chemistry techniques were utilized to elucidate the structure, and the results provided strong confirmation that the proposed structure indeed belongs to the category of MOFs. The synthesized In-MOF microcrystals were employed to remove dyes from contaminated water, where typical concentrations ranged from 1 to 50 parts per million (ppm). The effectiveness of the process was evaluated through kinetic and thermodynamic studies. The application of In-MOF microcrystals presents a promising and effective remedy for treating water polluted with harmful dyes. Through the elimination of these dyes, this innovative material has the potential to safeguard the integrity of the natural environment and mitigate adverse impacts on the ecosystem. The adsorption results reveal that In-MOF exhibits remarkable selectivity towards MB, AZA, AZB, and TOLO, and even in the presence of RHB, it exclusively removes MB, indicating its high specificity for this dye. Although the synthetic strategy for In-MOF shows promise for scaling up for industrial dye removal, there may be obstacles to overcome before it can be practically implemented. Presently, In-MOF synthesis has only been demonstrated on a gram scale and further research is needed to determine its feasibility for large-scale production.

Experimental section

Materials and methods

All of the chemical reagents and solvents utilized in this study were obtained commercially and employed directly without further purification. The chemicals used in this study include Benzene-1,2,4,5-tetracarboxylic acid (H_4BTA), Indium(III)nitrate monohydrate ($In(NO_3)_3 \cdot H_2O$), Diethylformamide (DEF), Nitric acid (HNO_3), Methylene Blue (MB), Azure A (AZA), Azure B (AZB), Toluidine Blue O (TOLO), Rhodamine B (RHB), and Congo red (CR) were obtained from Sigma Aldrich (India), TCI and Spectrochem.

The phase structure of materials at room temperature was analyzed using X-ray diffraction (XRD) patterns obtained on a PAnalytics X-ray diffractometer with a Cu $K\alpha 1$ radiation source ($\lambda = 0.15406$ nm) at an acceleration voltage of 40 kV and a current of 40 mA, over a 2θ range of 5 to 80°. Fourier transform infrared (FTIR) spectra were obtained using a SHIMADZU spectrophotometer in the range of 4000 to 400 cm^{-1} . The morphology and size of the materials were studied using Field emission transmission electron microscopy (FE-SEM) on a Mira3 Tascan-xmu instrument. The chemical composition of the materials was analyzed using Elemental Analysis (Thermo Fisher Scientific) and the presence of metal was determined using Inductively Coupled Plasma Optical Emission Spectroscopy (ICP-OES) on an AVIO-200 (Perkin Elmer) instrument. The specific surface area and pore size of the materials were determined using N_2 adsorption–desorption isotherms and Brunauer–Emmett–Teller (BET) techniques on a BELSORPmini II surface area and a pore size analyzer. The thermal stability of the materials was characterized using thermogravimetric analysis (TGA) on a TA Module Q 600 instrument under an N_2 atmosphere at a heating rate of 10 $^\circ C/min$. The absorption spectra of the materials were obtained using a UV–Vis spectrophotometer.

Synthesis of $[In_2(BTA)_2 \mu\text{-}NO_3 \cdot 8H_2O]$ in glass vial (1)

In-MOF was synthesized by dissolving $In(NO_3)_3 \cdot H_2O$ (23 mg, 0.0764 mmol) and H_4BTA (10 mg, 0.0393 mmol) in the mixture of DEF (1 mL) and distilled water (0.5 mL) with the addition of HNO_3 (3.6 M in DEF, 0.2 mL). The solution was then sealed in a 20 mL glass vial and sonicated for 30 min (Fig. S2). The mixture was subsequently heated in an oil bath at 85 $^\circ C$ for 8 h to facilitate crystal formation. The resulting white microcrystals were cooled to room temperature and washed with DEF, acetone, and DI (Deionised) water to remove any leftover impurities. The crystals were then activated by immersing them in MeOH for 72 h at 60 $^\circ C$, with fresh MeOH being replaced every 8 h. The final step involved drying the product for 24 h under high vacuum conditions. Yield: 0.015 g, 47% (based on H_4BTA).

Synthesis of $[\text{In}_2(\text{BTA})_2\mu\text{-NO}_3\cdot 8\text{H}_2\text{O}]$ in round bottom flask (RBF) and oil bath (2)

In order to synthesize In-MOF in RBF, a mixture of $\text{In}(\text{NO}_3)_3\cdot\text{H}_2\text{O}$ (1.18 g, 3.92 mmol) and H_4BTA (0.500 g, 1.96 mmol) was dissolved in a mixture of DEF (45 mL) and distilled water (22 mL) along with the addition of HNO_3 (3.6 M in DEF, 8.7 mL). The resulting solution was then sonicated in RBF for 30 min and heated in an oil bath at 85 °C for 8 h (Fig. S3). The resulting white microcrystals were cooled to room temperature and subsequently washed with DEF, acetone, and deionized water. The sample was then subjected to an activation procedure by immersion in MeOH for 72 h at 60 °C, wherein MeOH was changed every 8 h. Finally, the product was dried in a high vacuum condition for 24 h. Yield: 0.858 g, 44% (based on H_4BTA).

Microwave-assisted synthesis of $[\text{In}_2(\text{BTA})_2\mu\text{-NO}_3\cdot 8\text{H}_2\text{O}]$ (3)

The synthesis of In-MOF using a microwave-assisted method involved transferring a solution of $\text{In}(\text{NO}_3)_3\cdot\text{H}_2\text{O}$ (1.18 g, 3.92 mmol) and H_4BTA (0.500 g, 1.96 mmol), HNO_3 (3.6 M in DEF, 8.7 mL) to a 50 ml reaction vessel. The vessel was then tightly sealed and placed in a microwave reaction system (Fig. S4). Synthesis was conducted at 85 °C with a heating rate of 20 °C/min for a reaction time of 30 min. Following the reaction, the extraction and activation processes were carried out in the same manner as described in the previous method. Yield: 0.936 g, 48% (based on H_4BTA).

Characterization of In-MOF

M.P. > 250 °C; IR data (cm^{-1}): 2990(b), 1550(s), 1375(s), 813(s), 705(s); elemental analysis calcd (%) for $\text{C}_{20}\text{H}_{20}\text{In}_2\text{NO}_{27}$: C, 25.66; H, 2.15; N, 1.50 found: C, 24.48; H, 2.81; N, 1.56; ICP-OES calcd (%) for In: In 24.53; found: In 25.00.

Stability of In-MOF (1 to 3)

The stability of In-MOF (1 to 3) in water is an important factor to consider in dye removal. To evaluate the stability of In-MOF in water, a process was developed that involved stirring 10 mg of In-MOF in 10 mL of water for 48 h at room temperature. After 48 h, the mixture was centrifuged to isolate the supernatant, which was then analyzed using ICP-OES to determine the concentration of indium and precipitate of In-MOF was dried in an oven at 50 °C and used for the PXRD. The results obtained from this analysis were used to evaluate the stability of In-MOF in water over 48 h. It is important to note that the stability of In-MOF can be influenced by various factors, including the solvent used, the temperature, and the duration of exposure to the solvent. Overall, the process developed in this study

provides a standard procedure for evaluating the stability of In-MOF in water, which can be useful in designing and optimizing applications of this material.

Preparation of dye-adsorbate

A 1000 ppm dye stock solution was diluted to create solutions with concentrations ranging from 10 to 50 ppm. For the purpose of kinetic analysis, the methylene blue (MB) dye was also diluted to concentrations ranging from 10 to 50 ppm. Neutral pH has been maintained for all the dye solutions.

Computational study

The geometries of the basic unit of In-MOF is optimized using the density functional theorem (DFT) along with Becke, 3-parameter, Lee–Yang–Parr (B3LYP) hybrid functional, and STO-3G* basis set. For the verification of stable geometry as well as energy calculations, frequency calculation was also performed at the same level of theory. All the optimizations and frequency calculations were performed using the Gaussian 09 package [52]. Whenever an imaginary frequency was observed for any geometry, the structure was again optimized using the tight convergence criteria. In order to account for the long-range electron correlation effects arising out of the non-covalent interactions, Grimme's dispersion correction with Becke–Johnson Damping (D3-BJ) was applied. Further, for studying the interaction of the cationic dyes, MB and RHB with In-MOF, the structures of the dyes, In-MOF, and complex were also optimized at DFT/B3LYP/3-21 G* level of theory. It is well established that for ionic structures, calculations using the B3LYP functional are able to predict energies accurately without any dispersion correction [53–57]. Hence, empirical dispersion correction was avoided. The MOF-dye interaction energy was calculated as:

$$\Delta E = E_{\text{complex}} - (E_{\text{MOF}} + E_{\text{dye}})$$

Results and discussion

Synthesis of In-MOF

This study successfully synthesized In-MOF microcrystals using three different methods: Glass vial, Round bottom flask (RBF), and Microwave-assisted (Fig. 1). While all three methods yielded desired results, the microwave-assisted approach demonstrated significant advantages in terms of reaction time reduction. The microwave method demonstrated its efficiency and rapidity in synthesizing In-MOF by significantly reducing the synthesis time from 8 h to just 30 min. The effectiveness of the microwave-assisted method can be attributed to its unique heating mechanism, which ensures uniform and efficient heating throughout the reaction mixture. This results in accelerated reaction kinetics, leading to shorter synthesis times. Such a reduction in reaction time not only enhances productivity but also provides

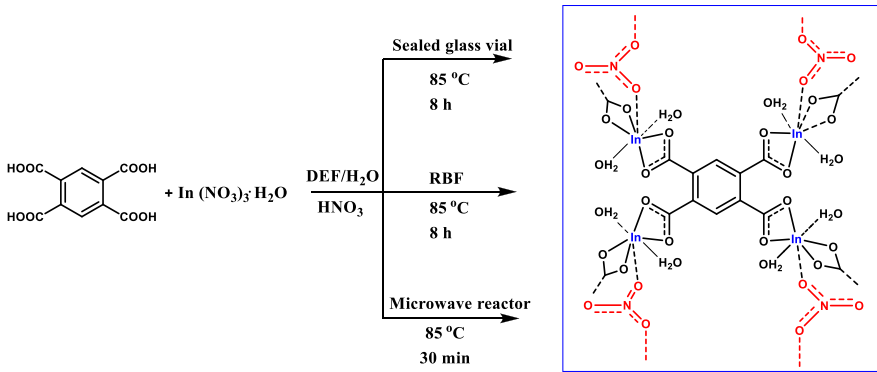


Fig. 1 Synthesis of In-MOF in different conditions

opportunities for scaling up the production of material. These results provide valuable insights into In-MOF synthesis and offer potential practical implications for the development of new and improved methods.

Indeed, various synthesis methods were employed for In-MOF, but they consistently resulted in the formation of microcrystals. Nevertheless, extensive efforts were undertaken to cultivate pristine single crystals of In-MOF inside glass vials with the ultimate goal of attaining a highly ordered and precisely defined crystalline structure. However, the outcome yielded a material with a microcrystalline nature characterized by poorly formed or disordered crystals. Consequently, the comprehensive characterization of the crystal structure was hampered. It is noteworthy that the synthesis of MOFs encompasses a diverse range of possibilities in MOF preparation. Different synthetic approaches can result in varied outcomes, including well-formed crystals with high structural integrity, as well as structures exhibiting disorder. In the specific case of the synthesized In-MOF, three different methods were employed, leading to a disordered structure devoid of well-arranged crystal structures or precise organizational patterns. Furthermore, Indium and H_4BTA have been utilized to prepare AUBM-1, MIL-117, and 3D In(III)-MOF using solvothermal and hydrothermal methods with autoclave [58–60], but none of these studies have explored microwave synthesis, gram-scale synthesis, or synthesis in an oil bath. Despite having the same metal and ligand, these MOFs exhibit distinct structures. The structural properties of the synthesized In-MOF microcrystals were analyzed using PXRD analysis. The analysis revealed a prominent and intense peak, which indicated its crystalline nature (Fig. 2b). The comparison of the obtained diffraction peaks from In-MOF with AUBM-1, MIL-117, and 3d In(III)-MOF (Fig. 2a) [58–60] indicates that In-MOF exhibits some structural similarities with AUBM-1, despite having different elemental compositions. To validate this, the PXRD data of In-MOF was processed using the HighScore Plus software by Panalytical, which is widely acknowledged for its proficiency in handling PXRD data. The analysis reveals that In-MOF shows the closest match with AUBM-1, while the other MOFs exhibit significantly distinct structural characteristics. Specifically, 17 out of 25 matching diffraction lines were

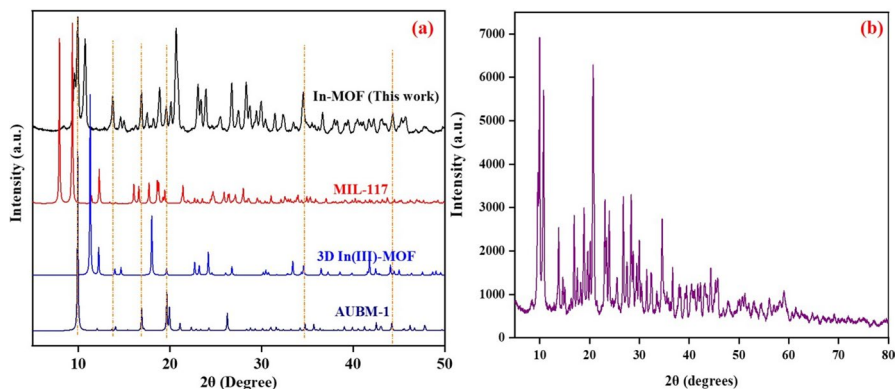


Fig. 2 **a** The XRD data comparison of AUBM-1, MIL-117, 3D In(III)-MOF, and In-MOF synthesized in a glass vial. **b** The XRD data of In-MOF synthesized in a glass vial

identified between In-MOF and AUBM-1, leading to a similarity score of 47 (with 100 representing a perfect match) (Fig. S12). These findings indicate both similarities and notable differences between the XRD patterns of In-MOF and AUBM-1, suggesting a certain degree of structural similarity. However, based on the comprehensive comparison and data processing, it can be concluded that AUBM-1, MIL-117, 3d In(III)-MOF, and In-MOF do not possess identical structures. Additional examination of the XRD data also indicates the existence of a metal oxide (In-O) linkage incorporated within the polymer framework of In-MOF, as evidenced by a peak observed at 30–50° 2θ in the XRD pattern. Moreover, the similarities in the XRD patterns with AUBM-1 suggest that the structure of In-MOF may exhibit a tetragonal crystal system. Comparing the XRD patterns of synthesized In-MOF using different methods, it is evident that they exhibit identical structures (Fig. S7).

FTIR data of an In-MOF material provide information about the different stretching modes in the structure of the material. The data have been used to compare the characteristics of the In-MOF synthesized using each strategy, such as the presence of certain functional groups. The FTIR spectra of In-MOF (**1** to **3**) revealed characteristic peaks of the carboxylate group of the MOF at 1580 cm^{-1} (method-1) 1574 cm^{-1} , (method-2) 1550 cm^{-1} (method-3) (Fig. 3). Notably, the spectra did not exhibit the carboxylic acid $\nu_{\text{C=O}}$ peak in the ligand at 1710 cm^{-1} . This is likely due to the formation of carboxylate anions, which results in the formation of a delocalized electronic cloud and the appearance of typical carboxylate peaks in the range of 1610 to 1550 cm^{-1} and 1420–1300 cm^{-1} . Additionally, peaks ranging from 880 to 730 cm^{-1} observed in the In-MOF spectrum may indicate the presence of In-O bonding [61]. These observations support that the desired coordination complex was generated by the metal salt and organic ligand.

In adsorption processes, the surface area and shape of the adsorbent are crucial factors that determine the efficiency of the adsorption. Scanning electron microscopy (SEM) is a technique used to observe the surface structure of materials at a high resolution. The data obtained from SEM can provide information on the size,

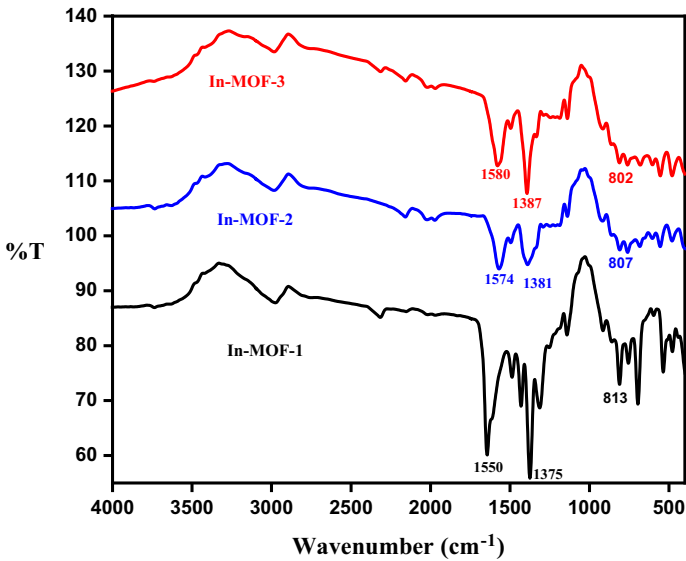


Fig. 3 The FTIR spectroscopy data has been collected for an In-MOF material synthesized through three distinct methods: 1 in a glass vial, 2 using a round-bottom flask (RBF), and 3 employing microwave-assisted synthesis

shape, and distribution of the particles in a material. Hence, to understand further the properties of the synthesized In-MOF, their morphology and microstructure were determined using SEM. As seen in Fig. 4a (synthesized in sealed glass vials) and S6 (synthesized in microwave conditions), these studies revealed that In-MOFs obtained from different methods have similar morphology, consisting of nano-scale crystals with a hollow needle-like shape (Fig. 4b). Moreover, additional images obtained at different resolutions showed that the In-MOFs exhibit a fiber cluster morphology, where small and long fibers combine to form clusters of small crystals (Fig. 4a–d). Furthermore, the SEM images of the In-MOFs microcrystals reveal a unique tubular structure formed by combining multiple microcrystals, allowing individual tubes to act as separate containers. This tubular structure suggests that the inner and outer surfaces of the tubes come into contact with dye molecules, which may lead to efficient encapsulation of the dye. The In-MOFs microcrystals demonstrate effective encapsulation of dye molecules within their tube-like structure, showcasing their potential as functional materials for diverse applications such as drug delivery and catalysis.

The elemental composition of the In-MOF was also determined using energy-dispersive X-ray spectroscopy (EDX), as shown in Fig. 4c. The results of this analysis showed the presence of In, O, C, and N elements, and no other contaminating peaks were detected. Overall, these results provide further insights into the properties of the synthesized In-MOF, which may aid in understanding its adsorption behavior and potential for practical applications.

The specific surface area, average pore diameter, and pore volume of In-MOF were determined using nitrogen adsorption–desorption isotherm experiments.

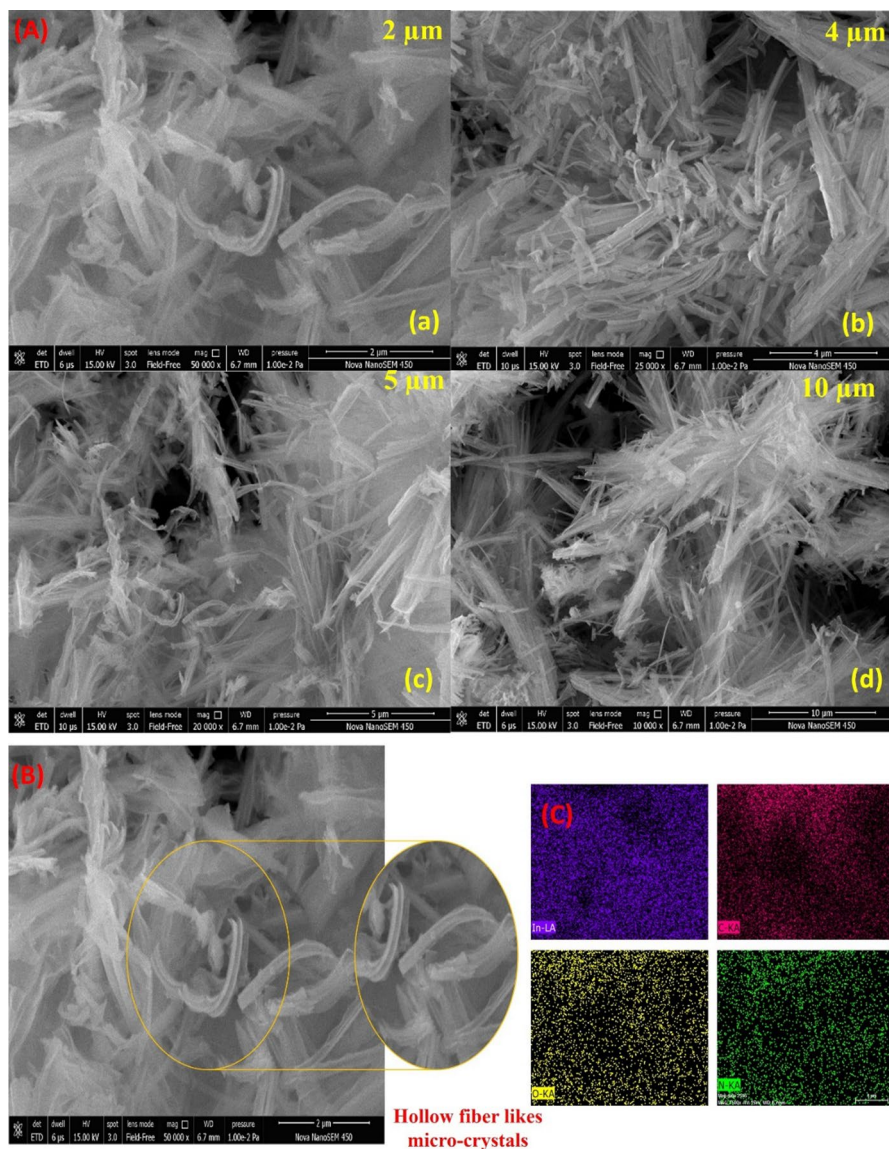


Fig. 4 **A** SEM images of In-MOF-1 synthesized in sealed glass vials. **B** Hollow needle-like microcrystals of In-MOF-1. **C** Energy-dispersive X-ray spectroscopy spectrum of In-MOF-1

The displayed isotherms indicate the presence of pores (3.37022 nm) within the material, which corresponds to a BET-specific surface area of $67.100 \text{ m}^2 \text{ g}^{-1}$ for the In-MOF. The low surface area observed could be attributed to the significant interpenetration of frameworks or the external area stemming from the relatively small crystal size. The presence of hysteresis during desorption, likely due to irreversible sorption of gas molecules on pore surfaces, suggests the presence of

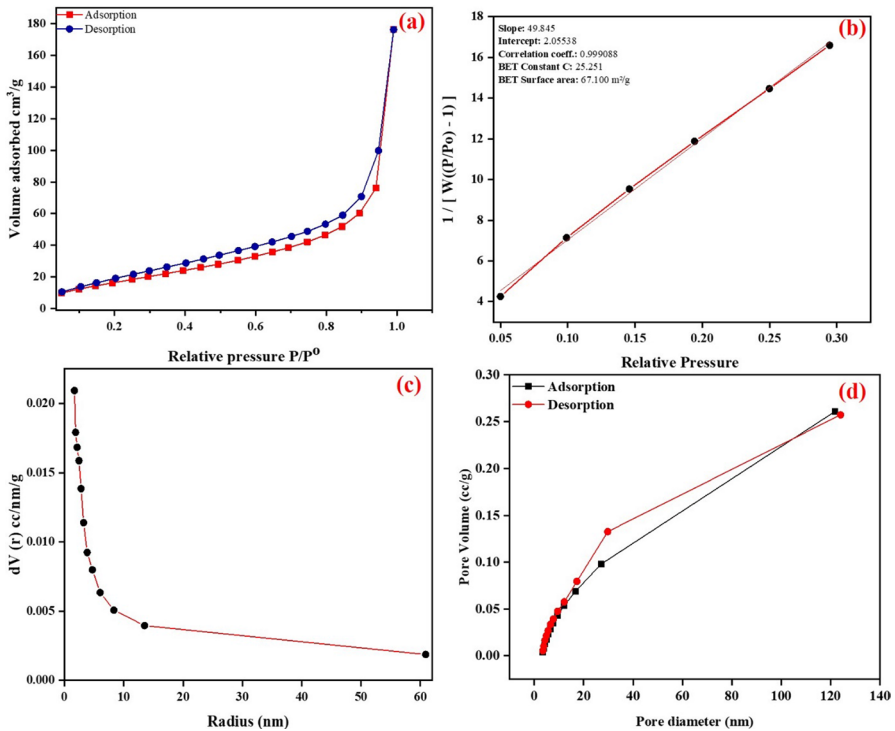


Fig. 5 **a** Nitrogen sorption isotherm measured at 77 K. **b** A BET fit was obtained using the low-pressure region data of the N_2 adsorption isotherm. **c** A plot of the pore radius vs. incremental pore area of In-MOF. **d** A plot of the Barrett–Joyner–Halenda (BJH) for adsorption and desorption pore size distribution

highly aggregated structures (Fig. 5a). Before conducting the isotherm measurements, the In-MOF-1 sample was degassed at 100 °C for 3 h. Furthermore, the pore size distribution curve computed using the Barrett–Joyner–Halenda (BJH) model. Figure 5d shows a slight curving trend with no distinguishable peaks. This In-MOF pore size distribution plot suggests a single mode for both the adsorption and desorption processes, with pore diameters of about 29.7 and 27.0 nm, respectively. Additionally, total pore volumes for adsorption and desorption are 0.26 cc/g and 0.25 cc/g, respectively. This curved pore distribution is caused by a narrow or uniform pore size distribution, in which the majority of pores are the same size. The BET isotherm exhibits type III behavior, indicating mesoporosity (Fig. 5a).

A thermogravimetric analysis (TGA) was performed on In-MOF, using a heating rate of 10 °C per minute within the temperature range of 30 to 800 °C. The experiment was conducted in a continuous flow of nitrogen gas. The thermogravimetric analysis (TGA) curve in Fig. 6a shows two major weight losses. The first weight loss of 28 wt% up to 300 °C is attributed to the removal of water and NO_3^- from the $[In_2(BTA)_2\mu-NO_3 \cdot 8H_2O]$ chemical formula. Theoretical calculations indicate that there is approximately 5.8 wt% of additional water

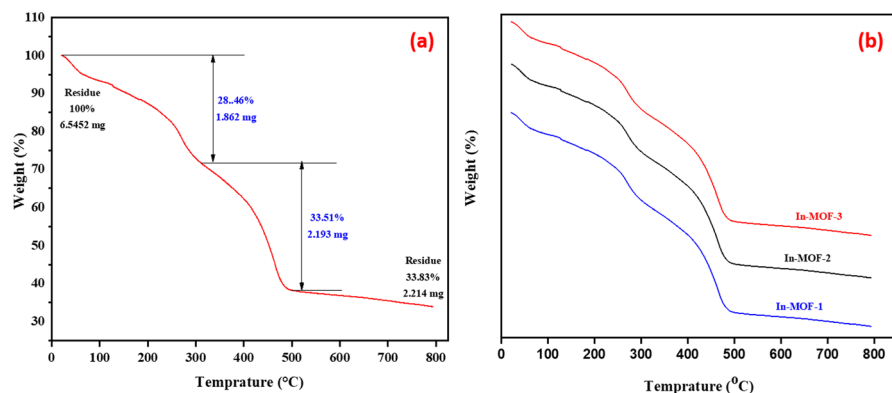


Fig. 6 a TGA graph of In-MOF. b TGA data comparison of In-MOF synthesized using various methods

adsorbed on the surface or trapped within the pores. The second weight loss of 33.5 wt% up to 500 °C is due to the decomposition of the benzenetetracarboxylate ligand and the removal of its fragments. The final residue of 33.83 wt% corresponds to indium oxide (In_2O_3). The calculated chemical formula from TGA is $[\text{In}_2(\text{BTA})_2\mu\text{-NO}_3\cdot 8\text{H}_2\text{O}]$ taking into account the first weight loss attributed to trapped water species. The thermal characteristics of In-MOF synthesized using three different strategies are found to be consistent or similar (Fig. 6b).

Furthermore, the elemental composition of the produced In-MOF was verified using elemental analysis and inductively coupled plasma-optical emission spectrometry (ICP-OES) was used for analyzing the composition of Indium (Table 1). By comparing the percentage of the elements determined from the elemental analysis and their theoretical values, the synthesized structures can be verified. Figure 8 displays a potential structure for In-MOF, where nitrate (NO_3) serves as a bridging ligand connecting different parts of the framework. Bridging ligands, are commonly found in many metal–organic frameworks, where they contribute to the stability and functionality of the material. There are several examples of MOFs that utilize bridging ligands, and some of these have been cited in the literature [62–65]. The computed values and the results of the elemental analysis supported the synthesis of the MOFs' structure. The slight imperfection of the experimental and theoretical values can be credited to the inaccuracy of the synthesized structure or the deposit of water molecules in the pores of the In-MOF.

In order to investigate the structural geometry of the In-MOF unit, a Density Functional Theory (DFT) study was conducted. This computational method was utilized to analyze and understand the arrangement and configuration of atoms within the In-MOF structure. The optimized geometry of the structural unit In-MOF is shown in Fig. 7.

Table 1 Elemental analysis and ICP-OES results

Sample		% C	% H	% N	% O	% In
In-MOF	Theoretical	25.66	2.15	1.50	46.15	24.53
	Experimental	24.48	2.81	1.56	45.75	25.00

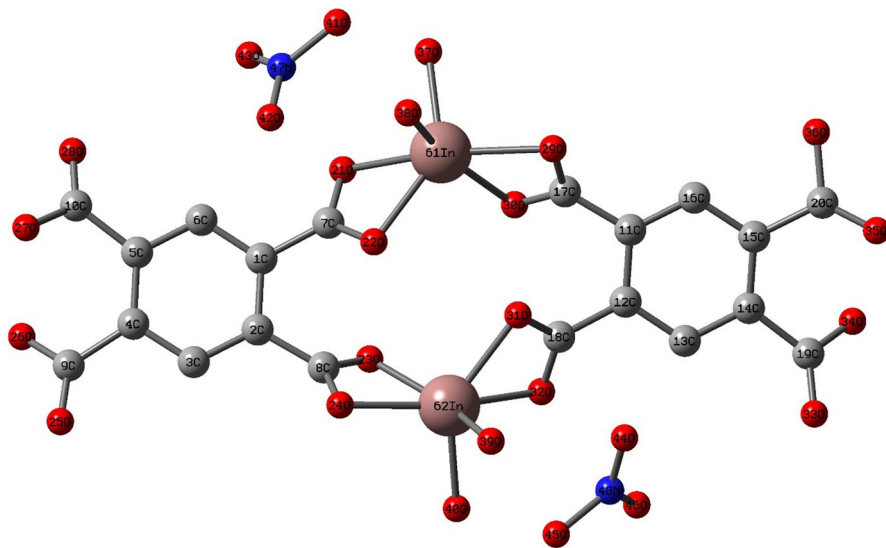


Fig. 7 Geometry of Indium –MOF optimized at DFT/B3LYP/3-21G* level of theory. For simplification and clarity purposes, the hydrogen atoms are not shown for clarity purposes

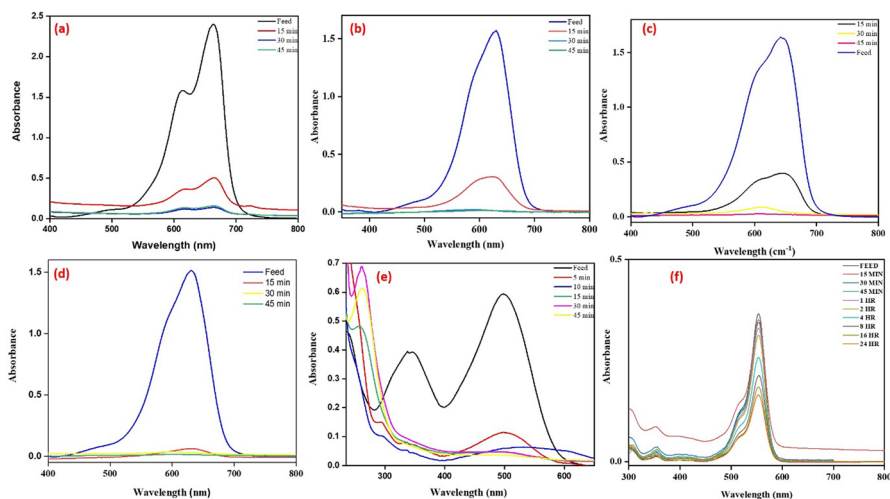


Fig. 8 UV – vis absorption spectra of **a** MB, **b** AZA, **c** AZB **d** TOLO **e** CR, and **f** RHB in water in the presence of In-MOF at different time intervals

The geometric parameters such as bond lengths, bond angles, and dihedral angles are summarized in Table S12. In the optimized structure, wherever water molecules are concerned, all the In-O bond lengths are in the range of 2.13–2.23 Å, which indicates strong interaction comparable to the In-O bond in Indium oxide [66]. Due to the small structure of the water molecules, they show stronger interaction with the Indium ion

leading to relatively shorter bond lengths ~ 2.13 – 2.15 Å. On the other hand, the movement of carboxylic O-atoms is more restricted as well as hindered due to steric factors, resulting in bond lengths of ~ 2.17 – 2.23 Å. The nitrate ions present in the lattice do not bind with the In(III) ions, however, they show weak interactions (bond length ~ 3.31 – 3.58 Å). In conclusion, the optimized geometry obtained from the DFT study aligns with the results from elemental analysis, PXRD, and ICP-OES data. Additionally, the structure of In-MOF exhibits certain similarities with AUBM-1, as confirmed by the processed PXRD data of these two materials.

Stability of In-MOF in water

In order to ensure the safety and effectiveness of technologies that involve the use of indium, it is crucial to assess its stability and solubility in water. This study investigated the stability and solubility of In-MOFs in water using ICP-OES and PXRD techniques. After 48 h of stirring in water, the In-MOFs were subjected to centrifugation, and the supernatant was analyzed using ICP-OES to determine the amount of indium remaining in the water. PXRD analysis was also performed on the precipitate to examine any changes in the In-MOFs crystal structure. The results showed that there was no residual indium in water after 48 h of stirring, indicating that the In-MOFs are highly stable and insoluble in water (Table S4). Furthermore, the PXRD analysis revealed that the crystal structure of In-MOFs remained intact (Fig. S8), demonstrating their ability to maintain their effectiveness in dye removal applications. The absence of residual indium in water after 48 h also suggests that In-MOFs do not dissolve in water, reducing the potential health risks associated with indium release into the environment. Overall, these findings suggest that In-MOFs are a safe and effective option for dye removal applications.

Batch dye adsorption experiment

The synthesised In-MOF has been explored for potential use in removing cationic organic dyes due to the tubular structure of In-MOF micro crystals and high water in-solubility and stability. Two critical elements that influence the selective dye adsorption of MOFs are the charge and size of organic dyes. The zeta potential of In-MOF refers to the surface charge of the material, and a negative zeta potential indicates that the surface of the material has a net negative charge. In-MOF have a negative zeta potential (-9.5 , Fig. S9), and they can interact with positively charged species, such as cationic dyes. The interaction between In-MOF and cationic dyes can result in the removal of the dyes from the solution. The dyes can be physically adsorbed onto the surface of the In-MOF. Overall, the negative zeta potential of In-MOF makes them effective at removing cationic dyes from solution through electrostatic interactions. The adsorption capacity of In-MOF was investigated using a variety of organic dyes, including Methylene Blue (MB), Azure A (AZA), Azure B (AZB), Toluidine blue O (TOLBO), Congo Red (CR), and Rhodamine B (RHB). The adsorption ability of In-MOF was assessed by monitoring the concentration changes of these dyes in water solutions at room temperature. In-MOF is highly

Table 2 Dye removal capacity of In-MOF over various cationic dyes

Adsorbent	Adsorbent mass (mg)	Dye	Dye concentration (mg/L)	Contact time (min)	Removal percentage (%)	Removal after the initial 15 min (%)
In-MOF	10 mg	MB	10 mg/L	45	98	77.87
		AZA		45	99	81.19
		AZB		45	98	75.81
		TOLO		45	99	95.80
		CR		240	93	80.95
		RHB		1440	82	4.01

Table 3 Comparison of MB removal capacity and initial contact time for In-MOF and other Adsorbents in recent studies

Adsorbent	Initial contact time (min)	MB removal efficiency (%)	Temperature	pH	References
SMGO	5 min	40	RT	–	[69]
PAMAM-functionalized Fe ₃ O ₄ @MOF	15 min	84	25–33 °C	8.4	[70]
OHC	10 min	42	s	–	[71]
Activated carbon developed from <i>Rumex abyssinicus</i>	20 min	82	RT	3	[72]
CeO ₂ -NPs/GO/PAM	15 min	45	RT	–	[73]
CuMn ₂ O ₄ /chitosan micro/nanocomposites	10 min	50	RT	6.5	[74]
In-MOF	15 min	80	RT	Neutral	This study

water insoluble which makes it easy to use in dye removal as well as provides practical applicability on an industrial scale. The adsorbent was stored in a desiccator and dried overnight at 100 °C under vacuum before adsorption. It was precisely weighed out and added to 10 mL of aqueous dye solutions with fixed dye concentrations of 10 mg/L. The dye solutions containing the adsorbents were well mixed with magnetic stirring and kept at room temperature for a predetermined amount of time (5 min to 24 h). The UV–vis absorption spectra of dye solutions at various periods throughout the adsorption process were noted.

The adsorption efficiency of In-MOF was evaluated using UV–vis spectrophotometry for a range of dyes including MB, AZA, AZB, TOLO, CR, and RHB which show characteristic absorption peaks at 664, 630, 640, 631, 497, and 550 nm, respectively (Fig. 8a to f). The adsorption kinetics were monitored over a period of 5 min to 24 h and the results showed a significant decrease in the dye concentration as well as a change in the color of the dye solutions and In-MOF microcrystals. The adsorption capacity of In-MOF was found to be high, with more than 75% (except RHB) removal efficiency of all dyes within 15 min (Table 2). Table 3 provides a

comparison of the dye removal capacity and initial contact time for In-MOF and other adsorbents in recent studies. Further, the pH-dependent adsorption behavior of MB onto In-MOF was also investigated across a wide pH range (2 to 14) (Fig. S12), revealing optimal removal efficiency within the pH range of 2 to 10 (~98%) but a notable decline at highly alkaline [pH = 12 (~37%) and pH = 14 (~23%)]. This decline can be attributed to a combination of factors, including pH-induced structural changes or degradation of In-MOF, competitive adsorption with hydroxide ions (OH⁻) at high pH, and alterations in the speciation of MB molecules, such as deprotonation, which results in reduced affinity for the MOF surface [67, 68]. These findings underscore the importance of considering pH effects when employing In-MOF for MB adsorption and have implications for optimizing their performance in diverse environmental and industrial applications involving solutions of varying pH levels.

Dye removal selectivity

Adsorption of mixed organic dyes onto In-MOF is observed using a method similar to that described above in order to examine the selectivity of In-MOF for dye adsorption. 10 mL of solution containing five dyes (10 mg/L for each dye) and 10 mg of as-synthesized In-MOF were combined. In the selectivity study, it was found that the In-MOF does not exhibit any preference for the removal of specific dyes among MB, AZA, AZB, and TOLO. When all four dyes were present in the same system, the In-MOF removed them in equal quantities within 45 min (Fig. 9a and b). However, when other dyes were present in the system, the In-MOF selectively removed

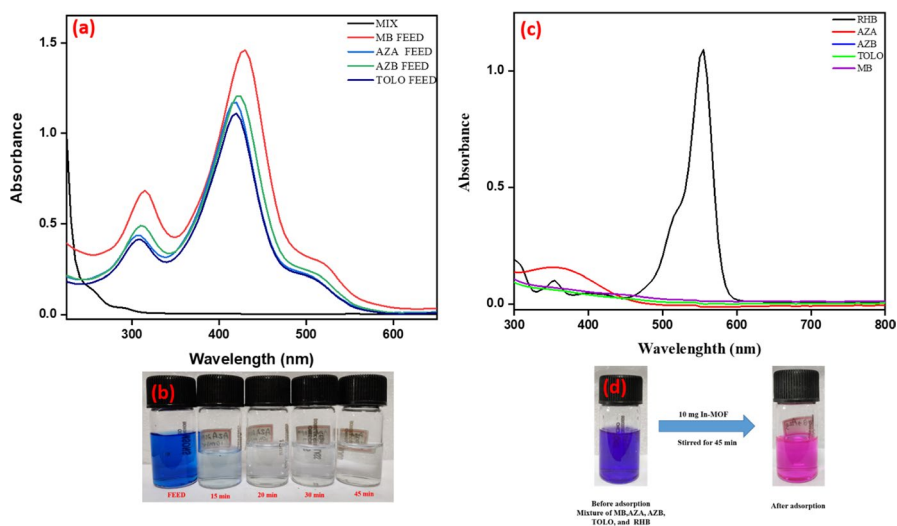


Fig. 9 a Dye removal of MB, AZA, AZB, and TOLO in one system b UV spectrum of mixed dye system with In-MOF. c Selectively removal of MB family. d UV spectra of selective removal of MB, AZA, AZB, and TOLO

only MB, AZA, AZB, and TOLO. This selectivity can be useful for removing the MB family of dyes from wastewater. To further demonstrate this selectivity, a study on a mixture solution of RHB with the MB family of dyes has been done, and the results showed that the In-MOF selectively removed only the MB family of dyes while leaving RHB unchanged (Fig. 10). The observed selectivity of the In-MOFs is attributed to the strong interaction between the In-MOF and the MB, AZA, AZB, and TOLO dyes, and the weaker interaction between the In-MOF and RHB.

Dye removal kinetics

The dye removal kinetics study is conducted to investigate the rate and mechanism, of how specific dyes from an aqueous solution have been removed by the adsorbent [75]. This study involves performing adsorption experiments at different initial concentrations of a dye and measuring the amount of dye removed over time [76–78]. By analyzing the data collected, it is possible to understand the mechanism of dye removal and determine the kinetic parameters of the adsorption process. In this study, 10 mL of an aqueous solution of MB with initial concentrations of 10 ppm has been taken. The applied kinetic models include the Pseudo-first-order kinetics

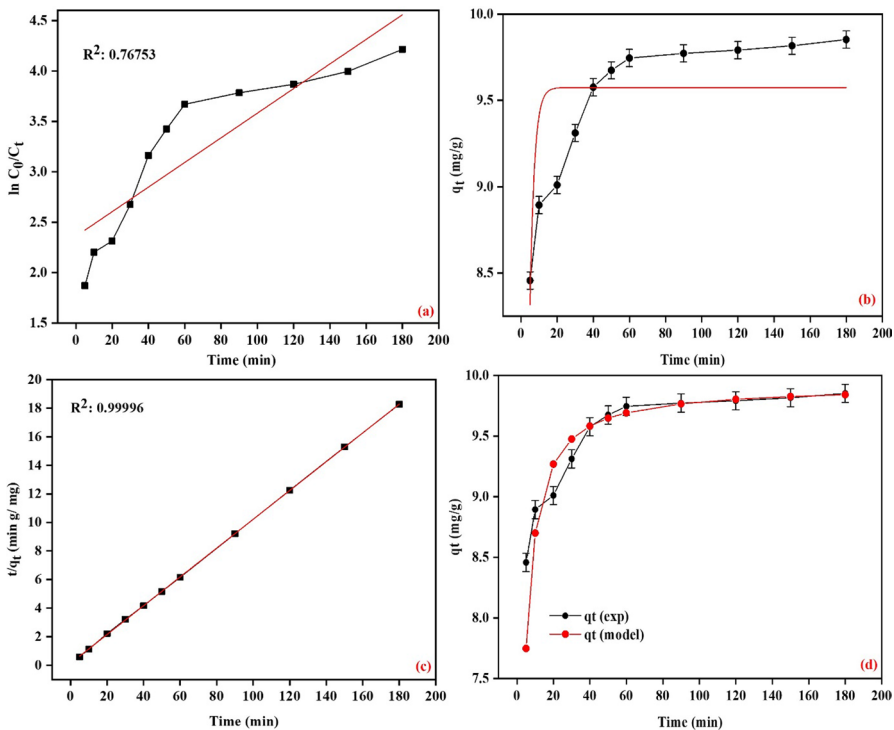


Fig. 10 a Pseudo first order graph: t vs $\ln C_0/C_t$. b Pseudo first order graph: t vs q_t . c Pseudo second order graph: t vs t/q_t . d Pseudo second order graph: t vs q_t

and Pseudo-second-order kinetics to understand the mechanism of dye removal and determine the kinetic parameters of the adsorption process [79, 80]. Other commonly used kinetic models in dye removal kinetics study are the Intraparticle diffusion model, and the Elovich model [81, 82].

Pseudo-first-order kinetics

The pseudo-first-order kinetic model is a commonly used method to describe the rate of adsorption [83, 84]. This model suggests that the adsorption rate is directly proportional to the concentration of the dye in the solution [85]. By plotting the graph of $\ln(q_e - q_t)$ against time (t) and analyzing the slope and correlation coefficient (R^2) of the data, the rate constant k_1 can be determined. A high R^2 value (close to 1) indicates a good fit for the kinetic model, but it is important to remember that this model assumes that the adsorption process is first-order and all adsorption sites are similar [86]. Therefore, it is recommended to compare the results obtained from the pseudo-first-order kinetic model with other kinetic models such as the pseudo-second-order kinetic model for a more accurate understanding of the adsorption process in real-world systems. The equation for the pseudo-first-order kinetic model is given by:

$$\ln(q_e - q_t) = \ln q_e - k_1 t$$

q_e = Amount of dye adsorbed at equilibrium (mg/g), q_t = Amount of dye adsorbed at time t (mg/g), k_1 = The pseudo-first-order rate constant (min^{-1})

The calculated equilibrium adsorption capacities do not agree with experimental values, because the R^2 value of the graph is not near the value of 1 ($R^2:0.76753$; Fig. 10a and b). This indicated that the adsorption of MB onto In-MOF is not an ideal pseudo-first-order reaction.

Pseudo-second-order kinetics

Unlike the pseudo-first-order kinetic model, the pseudo-second-order kinetic model assumes that the adsorption rate is directly proportional to the product of the concentration of the dye in the solution and the adsorbent surface area [87, 88]. The equation for the pseudo-second-order kinetic model is given by:

$$q_t = \frac{k_2 t q_e}{1 + k_2 t}$$

q_e = Amount of dye adsorbed at equilibrium (mg/g), q_t = Amount of dye adsorbed at time t (mg/g), k_2 = The pseudo-second-order rate constant (g/mg min)

The rate constant k_2 for adsorption kinetics can be determined by plotting t/q_t against t , as shown in Fig. 10c. The slope of this plot gives the value of k_2 and the correlation coefficient (R^2) can be used to determine how well the data fit with the kinetic model (Fig. 10d). The adaptable pseudo-second-order kinetic model is commonly used to analyze changes in the adsorbed amount over time. This model can provide insight into the adsorption process and is particularly useful

for comparing different adsorption kinetics. The parameters obtained from the slope and intercepts of the plot has been represented in Table S1. It was observed that the R^2 (0.99996) values for the pseudo-second order kinetics were greater than those for the pseudo-first kinetic model, indicating that the pseudo-second order kinetic model is more suitable for describing the adsorption process. This suggests that the adsorption of the MB dye by the In-MOF adsorbent is controlled by chemisorptions.

Adsorption isotherm

Adsorption isotherms are used to understand and plan the interaction between adsorbent and adsorbate at equilibrium [89, 90]. These isotherm models are mathematical equations that describe the relationship between the adsorption capacity of an adsorbent and the equilibrium concentration of the adsorbate, such as a dye, in a solution [91]. These models are used to predict the adsorption behaviour of a system under specific conditions. In this study, isotherms were determined by adding 10 mg of In-MOF to 10 mL of a dye solution with varying concentrations, ranging from 2 to 50 ppm. The mixture was then placed in stirring condition for 45 min and centrifuged before measuring the absorbance and the produced data have been used to compute the isotherm models.

The Langmuir isotherm

The Langmuir and Freundlich models were utilized to design the adsorption of MB onto In-MOF, and the corresponding parameters of each model were determined through regression analysis [92]. In general, the Langmuir model is represented by:

$$q_e = q_{max} \times \frac{K_l \times C_e}{(1 + K_l \times C_e)} \quad (1)$$

q_e = Dye adsorbed per mass of adsorbent, q_{max} = Maximum dye adsorption capacity, K_l = Langmuir constant, C_e = Dye concentration at equilibrium

Linear transformation of Eq. (1) gives Eq. (2), which is employed to determine the Langmuir isotherm constants q_{max} (mg/g) and b .

$$\frac{C_e}{q_e} = \frac{1}{q_{max}K_l} \times \frac{C_e}{K_l} \quad (2)$$

A graph was drawn between C_e/q_e and C_e , and the constants q_{max} and K_l were obtained from the slope and intercept (Fig. 11a). The data for the MB adsorption by In-MOF was modeled using the Langmuir isotherm ($R^2 = 0.99981$). The maximum adsorption capacity (q_{max}) and the Langmuir constant were calculated as 18.55 mg/g and 3.54, respectively (Table S2). The experimental adsorption capacity (q_{max}) matched closely with the calculated q_{max} (18.62 mg/g; Fig. 11b).

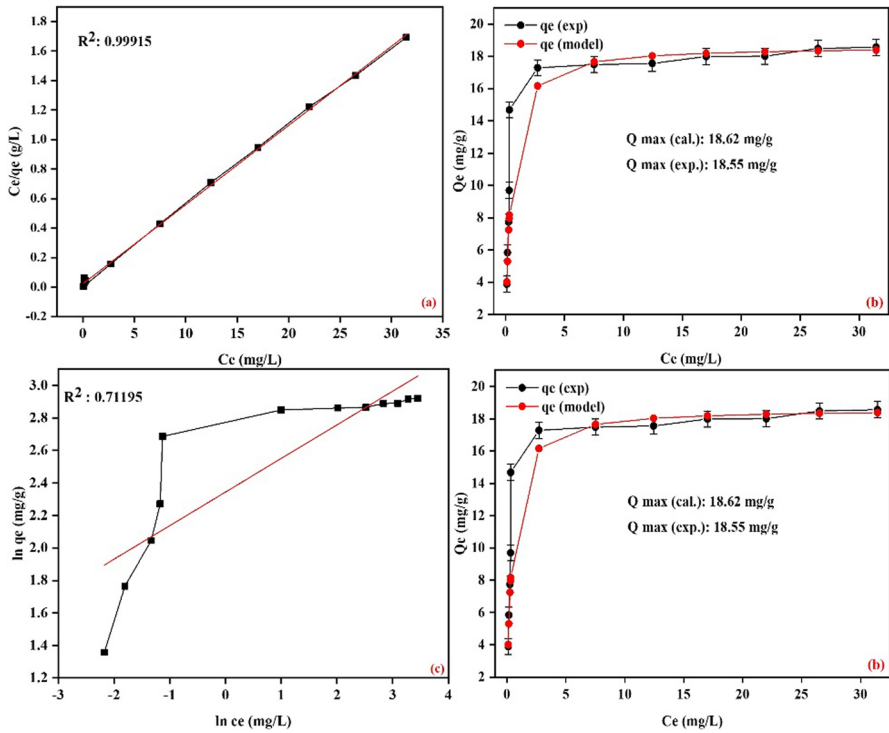


Fig. 11 **a** Langmuir isotherm graph of C_e vs C/q_e . **b** Langmuir isotherm graph of C_e vs q_e . **c** Freundlich isotherm graph of $\ln C_e$ vs $\ln q_e$. **d** Freundlich isotherm graph of C_e vs q_e

The Freundlich Isotherm

The Freundlich isotherm model, a nonlinear model, was utilized to evaluate the interaction between the adsorbate and the active sites of the adsorbent over a broad range of adsorbate concentrations [93]. This model enables the investigation of the surface heterogeneity of the adsorbent. It is represented as:

$$q_e = K_f C_e^{1/n} \tag{3}$$

K_f = Freundlich constant.

The linearized form of (3) is represented in Eq. (4) which is used to estimate the Freundlich isotherm constants.

$$\log q_e = \log K_f + \frac{1}{n \log C_e} \tag{4}$$

The linearized form of the Freundlich model equation (Eq. 4) was used to estimate the constants of the isotherm, K_f and n . The plot of $\log q_e$ vs. $\log C_e$ resulted in a straight line with a slope $(1/n)$ and intercept $(\log K_f)$ (Fig. 11c). The estimated constants, K_f and n , were presented in Table S2, and the fitted isotherm was shown in

Fig. 11d. The value of the slope ($1/n$) ranges between 0–1 and is used to determine the surface heterogeneity of the adsorbent. A low value of the slope indicates a high degree of heterogeneity. In this study, the value of the slope obtained was 0.20684, indicating that the surface of In-MOF is heterogeneous. Furthermore, the obtained values of K_f (10.42) and n (4.83) indicate that the adsorption of the organic dye over In-MOF is heterogeneous.

These results of the dye removal study revealed that In-MOF exhibits a high adsorption efficiency for the dyes, including methylene blue (MB), azure A (AZA), azure B (AZB), toluidine blue O (TOLBO), congo red (CR) and rhodamine B (RHB). The adsorption kinetics of the dyes were found to conform to the pseudo-second-order kinetic model, indicating that the adsorption process is controlled by chemisorption. The experimental data was also analyzed using the Langmuir and Freundlich isotherm models, which revealed that the adsorption process followed the Langmuir isotherm model, indicating that the adsorption process is monolayer adsorption and the adsorption capacity of In-MOF increases with an increase in the initial dye concentration. This suggests that In-MOF has a high potential as an adsorbent for the removal of cationic organic dyes from wastewater. To enhance our comprehension of the selectivity of MB (methylene blue) in the presence of RHB (rhodamine B), supplementary analyses were conducted employing pseudo-first-order and second-order kinetic models (Fig. S9), as well as Langmuir and Freundlich isotherm models (Fig. S10).

Adsorption isotherms and dye removal kinetics for RHB adsorption over In-MOF

The outcomes of the kinetic investigation demonstrate that the adsorption of RHB onto the In-MOF deviates from the pseudo-first-order and second-order models (Fig. S10), as indicated by the R^2 values of 0.95121 and 0.97721, respectively. This observation suggests that the adsorption of RHB onto the In-MOF material transpires at a sluggish pace. Additionally, the isotherm examination (Fig. S11) reveals that the adsorption of RHB adheres to the Langmuir isotherm model, substantiated by the high R^2 value approximating 1. This finding implies that the adsorption process of RHB onto the In-MOF material occurs as a monolayer adsorption process. Moreover, the adsorption capacity of In-MOF augments with increasing initial dye concentration, consistent with the predictions of the Langmuir model. Conversely, the Freundlich model displays a relatively inadequate fit, with an R^2 value of 0.507094, suggesting its unsuitability in describing the adsorption behavior of RHB on the In-MOF material. These findings provide valuable insights into the kinetics and isotherm of RHB adsorption, emphasizing the gradual adsorption kinetics and monolayer adsorption characteristics.

Proposed dye removal mechanism

Adsorption is a process in which molecules or particles like to adhere to a surface [94]. The In-MOF dye removal mechanism exhibits several robust potential pathways. One possible explanation is that electrostatic interactions between the cationic

dye and the negatively charged surface of the adsorbent play a vital role in the adsorption. Additionally, other potential interactions, such as hydrogen bonding and π - π stacking between the benzene ring of the adsorbent and the dye molecule, cannot be ruled out. Another explanation involves the concept of host-guest interactions in the context of dye removal. In this scenario, In-MOF acts as host, drawing in and capturing dye molecules, which act as the guests. These interactions may manifest through physical adsorption forces or chemical bonding, ultimately leading to the efficient elimination of dye from the MB solution. Overall, the adsorption mechanism is intricate, and to provide a more in-depth explanation of the interaction between cationic dyes MB and RHB with In-MOF, a computational study is utilized.

The optimized geometry of the In-MOF complexes with MB and RHB are shown in Fig. 12a and b, respectively. The hydrogen bond interactions between the MOF and the dyes are also shown in Fig. 12. It can be easily concluded that there are a

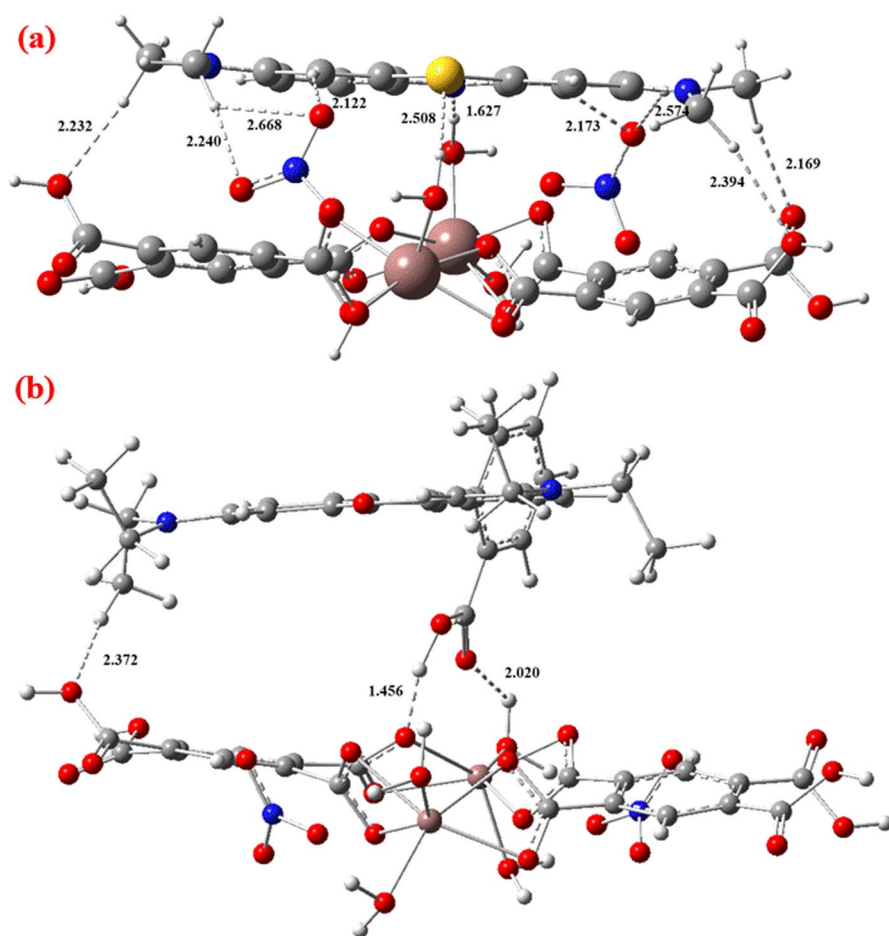


Fig. 12 Proposed mechanism of MB and RHB over In-MOF (single unit without NO_3^- linkage) surface

Table 4 Energy Table for the MOF-dye complex (E_{complex}), MOF (E_{MOF}) and dye (E_{dye})

E_{complex} (in Hartree units)	E_{MOF} (in Hartree units)	E_{dye} (in Hartree units)	ΔE (in Hartree units)	ΔE (in kcal/mol)
$E_{\text{MOF-MB}} = -15,432.954442$	$-14,256.604027$	$E_{\text{MB}} = -1176.287606$	-0.062787	-39.40
$E_{\text{MOF-RHB}} = -1568.899542$	$-14,256.604027$	$E_{\text{RHB}} = -1412.310972$	-0.015457	-9.70

lot of hydrogen bond interactions in the MB complex to that of the RHB complex (Fig. 12). Furthermore, it is also clearly visible that the dangling benzoic acid moiety in case of RHB hinders the approach of the cationic dye towards the In-MOF, resulting in less interactions. Again, from the difference in interaction energy of the two complexes (Table 4), it is quite evident that the In-MOF and RHB complex is a weak complex when compared to the In-MOF and MB complex. The less negative value (-9.70 kcal/mol) of the interaction energy for the In-MOF and RHB complex indicates that the complex is less stabilized. Conversely, for the In-MOF and MB complex, the theoretically calculated interaction energy is -39.70 kcal/mol which also supports the multiple hydrogen bond interaction within the complex. In conclusion, the computational study validates and elucidates In-MOF's significant selectivity for MB while also demonstrating its comparatively lesser adsorption capability for RHB.

Reusability of In-MOF in MB removal

A re-generable adsorbent can be cost-effective and in compliance with green chemistry. To do this, the dye was first removed from the exhausted adsorbent using 0.01 M HCl, and then the adsorbent was activated using MeOH. The procedure was repeated six times, and further dye removal investigations were carried out (Fig. 13). After subjecting In-MOF to a 0.01 HCL wash, a PXRD analysis was conducted which revealed that the structure of In-MOF remained unaffected (Fig. S5).

Even after the initial four successive regeneration trials, the percentage of dye removal remained higher than 90%. Thus, the In-MOF can be regarded as a superior reusable adsorbent in light of the findings.

Significance of using In-MOF as an adsorbent in dye removal

Some important significances of In-MOF use as adsorbent are listed below:

- In-MOF is relatively easy to synthesize, which makes it a desirable option for a wide ranges of applications.
- In-MOF can be synthesized using microwave technology, which is a green chemistry approach that can reduce the use of harmful chemicals and energy consumption.

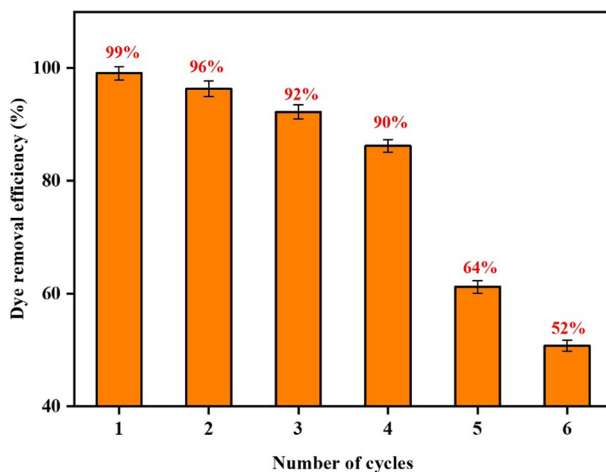


Fig. 13 Reusability of In-MOF for MB removal

- In-MOF has high removal efficiency for cationic dyes, making it useful for water treatment applications.
- In-MOF is highly water-insoluble, which makes it easy to recover after adsorption, reducing waste and increasing the efficiency of the process.
- It has high reusability, which makes it a cost-effective option for long-term use in various applications.

Several adsorbents have been developed in recent years for dye separation and purification, but some of them have limitations that can impact their effectiveness and practicality in certain wastewater treatment. In-MOF is a new and promising adsorbent with advantages such as high selectivity, good capacity, and good stability. In-MOF can overcome the limitations of other adsorbents (Table S6).

Conclusion

A new environmentally non-toxic In-MOF microcrystals was synthesized using three simple synthetic routes which have excellent adsorption capability for a variety of dyes, both individually and collectively in a solution. The adsorption results of the study showed that In-MOF has excellent removal efficacy for various dyes including Methylene Blue, Azure A, Azure B, Toluidine Blue O, Rhodamine B, and Congo Red. Additionally, it selectively removes certain dyes when present in a mixture. The adsorption kinetics and reusability of In-MOF studies suggest that it is appropriate for industrial applications due to its higher removal efficiency and adaptable synthetic pathway. In conclusion, while the synthetic strategy for In-MOF appears to be a promising method for scaling up to bulk production for industrial dye removal, it faces practical obstacles that need to be overcome. Currently, the

synthesis of In-MOF has only been successfully demonstrated on a gram scale, and further research is needed to determine its feasibility for large-scale production.

Supplementary Information The online version contains supplementary material available at <https://doi.org/10.1007/s11164-023-05161-w>.

Author Contributions K.M. has done all the experimental studies and designed the entire draft, A.K.G. performed the computational studies, S.K. and R.J. mentored the entire work and given approval for the final version of the manuscript.

Funding R. J. thanks SERB (project no. SRG/2021/000020) and Gujarat Council on Science & Technology (project no. GUJCOST/STI/2021-22/3877) for providing financial support and S. K. thanks the Director, Sardar Vallabhbhai National Institute of Technology Surat (Gujarat), for providing SEED GRANT for the research. K. M. is thankful to the SVNIT Surat for providing a fellowship for his research work.

Data Availability The supplementary information contains the data that supports the findings of the study.

Declarations

Conflict of interests The authors declare that they have no known competing financial interests or personal relationships that could have appeared to influence the work reported in this paper.

Ethical approval Not applicable.

References

1. I. Ali, Chem. Rev. **112**, 5073 (2012)
2. S.V. Kamath, M.H. Mruthunjayappa, D. Mondal, N. Sanna Kotrappanavar, Environ. Sci. Nano **9**, 2320 (2022)
3. A. Karmakar, A. Paul, I.R.M. Santos, P.M.R. Santos, E.P. Sabatini, A.V. Gurbanov, M.F.C. Guedes da Silva, A.J.L. Pombeiro, Cryst. Growth Des. **22**, 2248 (2022)
4. S. Kanan, M. Moyet, K. Obeideen, Y. El-Sayed, A.A. Mohamed, Res. Chem. Intermed. **48**, 3633 (2022)
5. J.A. Vanegas, Environ. Sci. Technol. **37**, 5363 (2003)
6. L. Singh, V.P. Singh, Microbial degradation of synthetic dyes in wastewaters, in *Springer International Publishing*, ed. by S.N. Singh (Cham, 2015), pp.187–204
7. R. Kishor, D. Purchase, G.D. Saratale, R.G. Saratale, L.F.R. Ferreira, M. Bilal, R. Chandra, R.N. Bharagava, J. Environ. Chem. Eng. **9**, 105012 (2021)
8. S. Thakur, A. Verma, V. Kumar, X. Jin Yang, S. Krishnamurthy, F. Coulon, V.K. Thakur, Fuel **309**, 122114 (2022)
9. R.R. Karri, G. Ravindran, M.H. Dehghani, in *Soft Computing Techniques in Solid Waste and Wastewater Management*, ed. R.R. Karri, G. Ravindran, M.H. Dehghani (Elsevier, 2021), pp. 3-33
10. J. Gong, J. Liu, X. Chen, Z. Jiang, X. Wen, E. Mijowska, T. Tang, J. Mater. Chem. A **3**, 341 (2015)
11. S. Manikandan, R. Subbaiya, M. Saravanan, M. Ponraj, M. Selvam, A. Pugazhendhi, Chemosphere **289**, 132867 (2022)
12. M.T. Yagub, T.K. Sen, S. Afroze, H.M. Ang, Adv. Colloid Interface Sci. **209**, 172 (2014)
13. A.K. Paul, J. Mol. Struct. **1125**, 696 (2016)
14. K. Maru, S. Kalla, R. Jangir, New J. Chem. **46**, 3054 (2022)
15. W. Liu, D. Sun, H. Ma, C. Ma, X. Zhang, J. Hao, Res. Chem. Intermed. **49**, 3161 (2023)
16. A. Shahzaib, A.I. Shaily, F. Zafar, S.M. Alshehri, S. Ali, N. Nishat, Res. Chem. Intermed. **49**, 2507 (2023)
17. A.R. Bagheri, N. Aramesh, F. Sher, M. Bilal, Chemosphere **270**, 129523 (2021)
18. Z. Li, L. Wang, J. Meng, X. Liu, J. Xu, F. Wang, P. Brookes, J. Hazard. Mater. **344**, 1 (2018)

19. A.A. Al-Gheethi, Q.M. Azhar, P. Senthil Kumar, A.A. Yusuf, A.K. Al-Buriah, R.M.S. Radin Mohamed, M.M. Al-shaibani, *Chemosphere* **287**, 132080 (2022)
20. H. Qiu, C. Liang, X. Zhang, M. Chen, Y. Zhao, T. Tao, Z. Xu, G. Liu, A.C.S. Appl. Mater. Interfaces **7**, 20835 (2015)
21. S. Biswas, J. Fatema, T. Debnath, T.U. Rashid, *ACS ES&T Water* **1**, 1055 (2021)
22. S. Talekar, Y. Kim, Y. Wee, J. Kim, *Chem. Eng. J.* **456**, 141058 (2023)
23. H. Figueiredo, C. Quintelas, *J. Hazard. Mater.* **274**, 287 (2014)
24. W. Gu, G. Yushin, *Wiley Interdiscip. Rev Energy Environ* **3**, 424 (2014)
25. M.R. Kasaai, *J. Agric. Food Chem.* **57**, 1667 (2009)
26. C. Montoro, D. Rodríguez-San-Miguel, E. Polo, R. Escudero-Cid, M.L. Ruiz-González, J.A.R. Navarro, P. Ocón, F. Zamora, *J. Am. Chem. Soc.* **139**, 10079 (2017)
27. B. Saha, S. Vedachalam, A.K. Dalai, *Fuel Process. Technol.* **214**, 106685 (2021)
28. X. Zhao, K. Wang, Z. Gao, H. Gao, Z. Xie, X. Du, H. Huang, *Ind. Eng. Chem. Res.* **56**, 4496 (2017)
29. S. Lin, Z. Song, G. Che, A. Ren, P. Li, C. Liu, J. Zhang, *Microporous Mesoporous Mater.* **193**, 27 (2014)
30. R. Gaillac, P. Pullumbi, K.A. Beyer, K.W. Chapman, D.A. Keen, T.D. Bennett, F.-X. Coudert, *Nat. Mater.* **16**, 1149 (2017)
31. A.F. Sapnik, I. Bechis, S.M. Collins, D.N. Johnstone, G. Divitini, A.J. Smith, P.A. Chater, M.A. Addicoat, T. Johnson, D.A. Keen, K.E. Jelfs, T.D. Bennett, *Nat. Commun.* **12**, 2062 (2021)
32. R. Aliakbari, S. Ramakrishna, E. Kowsari, Y. Marfavi, Z.A. Cheshmeh, F.B. Ajdari, Z. Kiaei, H. Torzkaban, M. Ershadi, *Res. Chem. Intermed.* **48**, 2767 (2022)
33. X. Zhao, C. Zhang, B. Liu, H. Zhao, X. Gao, Y. Wang, Y. Zhang, D. Liu, C.C. Wang, *Resour. Conserv. Recycl.* **188**, 106647 (2023)
34. P. Zhao, S.E. Tsang, D. Fairen-Jimenez, *Cell Rep. Phys. Sci.* **2**, 1 (2021)
35. N.A. Khan, Z. Hasan, S.H. Jung, *Coord. Chem. Rev.* **376**, 20 (2018)
36. R.A. Dodson, A.J. Matzger, *A.C.S. Mater. Lett.* **1**, 344 (2019)
37. J. Fonseca, T. Gong, L. Jiao, H.-L. Jiang, *J. Mater. Chem. A* **9**, 10562 (2021)
38. T.D. Bennett, A.K. Cheetham, *Acc. Chem. Res.* **47**, 1555 (2014)
39. C. Altintas, G. Avci, H. Daglar, A. Nemati Vesali Azar, S. Velioglu, I. Erucar, S. Keskin, *J. Mater. Chem. A* **7**, 9593 (2019)
40. T. Yang, T. Willhammar, H. Xu, X. Zou, Z. Huang, *Nat. Protoc.* **17**, 2389 (2022)
41. F. Rouhani, P. Mousavifard, *Sep. Purif. Technol.* **320**, 124230 (2023)
42. V. Kumar Maka, P. Tamuly, S. Jindal, J. Narasimha Moorthy, *Appl. Mater. Today* **19**, 100613–101135 (2020)
43. E. Haque, J.W. Jun, S.H. Jung, *J. Hazard. Mater.* **185**, 507 (2011)
44. F. Ahmadijokani, H. Molavi, M. Rezakazemi, T.M. Aminabhavi, M. Arjmand, *Coord. Chem. Rev.* **445**, 214037 (2021)
45. A.O. Ibrahim, K.A. Adegoke, R.O. Adegoke, Y.A. AbdulWahab, V.B. Oyelami, M.O. Adesina, *J. Mol. Liq.* **333**, 115593 (2021)
46. O. Ejeromedoghene, O. Oderinde, M. Kang, S. Agbedor, A.R. Faruwa, O.M. Olukowi, G. Fu, M.O. Daramola, *Environ. Sci. Pollut. Res.* **27**, 42346 (2020)
47. M. Firoozi, Z. Rafiee, K. Dashtian, *ACS Omega* **5**, 9420 (2020)
48. D. Karadag, E. Akgul, S. Tok, F. Erturk, M.A. Kaya, M. Turan, *J. Chem. Eng. Data* **52**, 2436 (2007)
49. G. Mezohegyi, F.P. van der Zee, J. Font, A. Fortuny, A. Fabregat, *J. Environ. Manage.* **102**, 148 (2012)
50. W. Cheng, Y. Wang, S. Ge, X. Ding, Z. Cui, Q. Shao, *Adv. Compos. Hybrid Mater.* **4**, 150 (2021)
51. X. Shi, Y. Zu, S. Jiang, F. Sun, *Inorg. Chem.* **60**, 1571 (2021)
52. M. Frisch, G. Trucks, H. Schlegel, G. Scuseria, M. Robb, J. Cheeseman, G. Scalmani, V. Barone, B. Mennucci, G. Petersson, in *Gaussian 09(Gaussian Inc Wallingford, 2009)*
53. P. Chatterjee, A.K. Ghosh, M. Samanta, T. Chakraborty, *J. Phys. Chem. A* **122**, 5563 (2018)
54. P. Chatterjee, A.K. Ghosh, T. Chakraborty, *J. Chem. Phys.* **146**, 84310 (2017)
55. M. Guo, H. Wu, M. Yang, Z. Luo, *J. Phys. Chem. A* **123**, 10739 (2019)
56. A.K. Ghosh, S. Datta, A. Mukhopadhyay, T. Chakraborty, *J. Phys. Chem. A* **117**, 8710 (2013)
57. A.K. Ghosh, A. Chattopadhyay, A. Mukhopadhyay, T. Chakraborty, *Chem. Phys. Lett.* **561–562**, 24 (2013)
58. H. Atallah, M. Elcheikh Mahmoud, A. Jelle, A. Lough, M. Hmadeh, *Dalton Trans.* **47**, 799 (2018)
59. M. Mazaj, C. Volkringer, T. Loiseau, V. Kaučič, G. Férey, *Solid State Sci.* **13**, 1488 (2011)
60. Z.B. Han, B.Y. Li, J.W. Ji, Y.E. Du, H.Y. An, M.-H. Zeng, *Dalton Trans.* **40**, 9154 (2011)

61. M. Khan, W. Khan, M. Ahamed, M. AlSalhi, T. Ahmed, *Electron. Mater. Lett.* **9**, 53 (2013)
62. S.K. Sachan, G. Anantharaman, *Inorg. Chem.* **60**, 9238 (2021)
63. S. Abednatanzi, P. Gohari Derakhshandeh, H. Depauw, F.X. Coudert, H. Vrielinck, P. Van Der Voort, K. Leus, *Chem. Soc. Rev.* **48**, 2535 (2019)
64. S. Yuan, Y.K. Deng, W.M. Xuan, X.P. Wang, S.N. Wang, J.M. Dou, D. Sun, *CrystEngComm* **16**, 3829 (2014)
65. X.J. Zhang, F.Z. Su, D.M. Chen, Y. Peng, W.Y. Guo, C.S. Liu, M. Du, *Dalton Trans.* **48**, 1843 (2019)
66. D.B. Buchholz, Q. Ma, D. Alducin, A. Ponce, M. Jose Yacaman, R. Khanal, J.E. Medvedeva, R.P.H. Chang, *Chem. Mater.* **26**, 5401 (2014)
67. L. Kong, Y. Wang, C.B. Andrews, C. Zheng, *Chem. Eng. J.* **435**, 134830 (2022)
68. S.A. Younis, N. Bhardwaj, S.K. Bhardwaj, K.H. Kim, A. Deep, *Coord. Chem. Rev.* **429**, 213620 (2021)
69. P. Kumari, N.M.K. Disha, D. Dhruwe, M.K. Patel, S. Mishra, *Ind. Eng. Chem. Res.* **62**, 1245 (2023)
70. Y. Heidari, E. Noroozian, S. Maghsoudi, *Sci. Rep.* **13**, 4924 (2023)
71. S. Madduri, I. Elsayed, E.B. Hassan, *Chemosphere* **260**, 127683 (2020)
72. J. Fito, M. Abewaa, A. Mengistu, K. Angassa, A.D. Ambaye, W. Moyo, T.N. Kambule, *Sci. Rep.* **13**, 5427 (2023)
73. Z. Kalaycıoğlu, B. Özüğür Uysal, Ö. Pekcan, F.B. Erim, *ACS Omega* **8**, 13004 (2023)
74. M. Samadi Kazemi, A. Sobhani, *Arab. J. Chem.* **16**, 104754 (2023)
75. M.S.U. Rehman, M. Munir, M. Ashfaq, N. Rashid, M.F. Nazar, M. Danish, J.I. Han, *Chem. Eng. J.* **228**, 54 (2013)
76. A.K. Yadav, P. Dash, A. Mohanty, R. Abbassi, B.K. Mishra, *Ecol. Eng.* **47**, 126 (2012)
77. P. Praipipat, P. Ngamsurach, A. Sanghuayprai, *Sci. Rep.* **13**, 1467 (2023)
78. M.A. Ahmed, M.A. Ahmed, A.A. Mohamed, *RSC Adv.* **13**, 5337 (2023)
79. R. Ahmad, R. Kumar, *Appl. Surf. Sci.* **257**, 1628 (2010)
80. Y. Zhang, L. Guo, M.R. Hoffmann, *ACS ES&T Eng.* **3**, 335 (2023)
81. F.C. Wu, R.L. Tseng, R.S. Juang, *Chem. Eng. J.* **150**, 366 (2009)
82. B.M. Al-Shehri, F.A.M. Al-Zahrani, R.M. El-Shishtawy, N.S. Awwad, M.A. Sayed, K.A. Khan, *Sci. Rep.* **13**, 1631 (2023)
83. W. Rudzinski, W. Plazinski, *J. Phys. Chem. C* **111**, 15100 (2007)
84. M. Loutfi, R. Mariouch, I. Mariouch, M. Belfaquir, M.S. ElYoubi, *Mater. Today: Proc.* **72**, 3638 (2023)
85. M.A.M. Salleh, D.K. Mahmoud, W.A.W.A. Karim, A. Idris, *Desalination* **280**, 1 (2011)
86. S. Nethaji, A. Sivasamy, *Chemosphere* **82**, 1367 (2011)
87. R.A. Shawabkeh, M.F. Tutunji, *Appl. Clay Sci.* **24**, 111 (2003)
88. N.S. Abdullah Sani, W.L. Ang, A.W. Mohammad, A. Nouri, E. Mahmoudi, *Sci. Rep.* **13**, 1931 (2023)
89. S. Chen, Q. Yue, B. Gao, X. Xu, *J. Colloid Interface Sci.* **349**, 256 (2010)
90. M. Rajabi, S. Keihankhadiv, I. Suhas, R.R. Tyagi, M. Karri, N.M. Chaudhary, S. Mubarak, P. Chaudhary, P.S. Kumar, *J. Nanostructure Chem.* **13**, 43 (2023)
91. A. Gil, F.C.C. Assis, S. Albeniz, S.A. Korili, *Chem. Eng. J.* **168**, 1032 (2011)
92. A. Ghosh, G. Das, *Microporous Mesoporous Mater.* **297**, 110039 (2020)
93. M.A. Al-Ghouti, D.A. Da'ana, *J. Hazard. Mater.* **393**, 122383 (2020)
94. X. Zheng, J. Zhang, J. Wang, X. Qi, J.M. Rosenholm, K. Cai, *J. Phys. Chem. C* **119**, 24512 (2015)

Publisher's Note Springer Nature remains neutral with regard to jurisdictional claims in published maps and institutional affiliations.

Springer Nature or its licensor (e.g. a society or other partner) holds exclusive rights to this article under a publishing agreement with the author(s) or other rightsholder(s); author self-archiving of the accepted manuscript version of this article is solely governed by the terms of such publishing agreement and applicable law.

Authors and Affiliations

Ketan Maru¹ · Sarita Kalla² · Arup K. Ghosh¹ · Ritambhara Jangir¹

✉ Ritambhara Jangir
ritambhara.jangir@chem.svnit.ac.in

Ketan Maru
ketanmaru61@gmail.com

Sarita Kalla
sarita_kalla@ched.svnit.ac.in

Arup K. Ghosh
akg@chem.svnit.ac.in

¹ Department of Chemistry, Sardar Vallabhbhai National Institute of Technology,
Ichchanath, Surat, Gujarat 395 007, India

² Department of Chemical Engineering, Sardar Vallabhbhai National Institute of Technology,
Ichchanath, Surat, Gujarat 395 007, India